Monthly Notices of the ROYAL ASTRONOMICAL SOCIETY

MNRAS **535,** 1439–1448 (2024) https://doi.org/10.1093/mnras/stae2425
Advance Access publication 2024 October 23

ExoMol line lists – LXII. Ro-vibrational energy levels and line strengths for the propadienediylidene (C_3) in its ground electronic state

A. E. Lynas-Gray,[1,2,3] O. L. Polyansky,[1,4] J. Tennyson ,[1]★ S. N. Yurchenko [1] and N. F. Zobov[4]

[1]*Department of Physics and Astronomy, University College London, Gower Street, London WC1E 6BT, UK*
[2]*Department of Physics, University of Oxford, Keble Road, Oxford OX1 3RH, UK*
[3]*Department of Physics and Astronomy, University of the Western Cape, Bellville 7535, South Africa*
[4]*Institute of Applied Physics, Russian Academy of Science, Ulyanov Street 46, Nizhnii Novgorod 603950, Russia*

Accepted 2024 October 22. Received 2024 October 21; in original form 2024 August 6

ABSTRACT

Improved opacities are needed for modelling the atmospheres and evolution of cool carbon-rich stars and extra-solar planets; in particular, contributions made by the astrophysically important propadienediylidene (C_3) molecule need, at a minimum, to be determined using a line list which includes all significant transitions in the energy range of interest. We report variational calculations giving ro-vibrational energy levels and corresponding line strengths for $^{12}C_3$, $^{12}C^{13}C^{12}C$, and $^{12}C^{12}C^{13}C$. In the $^{12}C_3$ case, we obtain 2166 503 ro-vibrational state energies $\leqslant$2000 cm^{-1} for the electronic $\tilde{X}\,^1\Sigma_g^+$ ground state. Comparison with experiment indicates a maximum error of $\pm$0.03 cm^{-1} in calculated positions of lines involving an upper state energy $\lessapprox$4000 cm^{-1}. For lines with upper state energies $\gtrapprox$4000 cm^{-1} to have comparable line-position accuracies, conical intersections would need to be accounted for in an adopted potential energy surface. Line lists and associated opacities are provided in the ExoMol data base (http://www.exomol.com).

Key words: molecular data – opacity – planets and satellites: atmospheres – stars: atmospheres – ISM: molecules.

1 INTRODUCTION

Interest in propadienediylidene (tricarbon, hereinafter C_3) follows the demonstration by Douglas (1951) that the molecular band near 4050 Å in cometary spectra may be attributable to it. First observed by Huggins (1881), the 4050 Å band is also seen in carbon star spectra (McKellar 1948) and work by Douglas allowed Swings, McKellar & Rao (1953) to identify C_3 as the carrier. A detection of C_3 is to be expected as Honig's (1954) determination of the dissociation energy (the energy required to break a C–C bond) of 160 kcal mol^{-1} (6.938 eV) led Tsuji (1964) to demonstrate that both C_2 and C_3 achieve maximum number densities in conditions prevailing in some carbon star atmospheres at temperatures $\lessapprox$2800 K.

Gausset et al. (1965) reproduced the C_3 4050 Å band in fluorescence and absorption using flash photolysis of diazomethane mixed with an excess (100:1) of nitrogen. The electronic transition $\tilde{A}\,^1\Pi_u - \tilde{X}\,^1\Sigma_g^+$ was found to produce the C_3 4050 Å band. Following their rotational analysis, Gausset et al. (1965) established through a vibrational analysis that there are two low lying $\tilde{X}\,^1\Sigma_g^+$ levels at 132 and 286 cm^{-1} which have to be respectively assigned as $2\nu_2$ and $4\nu_2$, leading to the discovery of the surprisingly low-order bending mode $\nu_2 \approx 64$ cm^{-1}.

Giesen et al. (2001) exploited the C_3 low-order bending mode to establish its presence in the interstellar medium along the line of sight towards Sgr B2(M). Reactions involving C_3 in the interstellar medium are understood to determine carbon chain abundances in dark clouds (Loison et al. 2014). Because C_2 and C_3 are obvious building blocks for larger carbon molecules such as C_{60}, Fan et al. (2024) located C_3 in a further 27 lines of sight for follow-up observations.

Hébrard et al. (2013) revised C_3-hydrocarbon models of Titan's atmosphere, finding C_3, c−C_3H, and C_3H_3 may be detectable. Results from high-dispersion optical spectroscopy (Rianço-Silva et al. 2024) are consistent with a C_3 column density of 10^{13} cm^2 in the upper atmosphere of Titan. An updated line list enabled Lombardo et al. (2019) to detect propadiene (CH_2CCH_2) in the atmosphere of Titan using infrared high-dispersion spectra; their spectra could also be used to search for C_3 were an adequate line list available.

Clayton (1996) reviewed R Corona Borealis (RCrB) stars whose atmospheric compositions are 99 per cent helium and 1 per cent carbon (by numbers); their light curves exhibit sharp and irregular decreases in brightness of roughly 6–8 mag, the original magnitude being recovered only after a slow increase in brightness which follows. Soot formation and dissipation in RCrB atmospheres is understood to be the cause of the characteristic RCrB light curves and it was therefore of some interest to note that laboratory studies of C_3 show it to be the dominant vapour species over graphite above $\approx$2000 K and identify it as a potential precursor for soot formation in flames (Goulay et al. 2010). Kameswara Rao, Giridhar & Ashoka (1990) identify the 4050 Å C_3 band in a RCrB spectrum obtained at maximum light and find it to have disappeared as minimum light is approached, suggesting that C_3 is now absent and soot formation has taken place.

★ E-mail: j.tennyson@ucl.ac.uk

Experiments by Weltner, Walsh & Angell (1964) and Weltner & McLeod (1964) respectively located the C_3 ground state asymmetric and symmetric stretches at 2040 and 1230 cm^{-1}. Gilra (1973) then argued that C_3 should be included as a contributor to a broad absorption feature seen in carbon star spectra at $\sim$5 μm and that it contributes significant opacity at this frequency. Treffers & Gilra (1975) studied the vibrational spectrum of C_3 in the $\sim$5 μm region, using a carbon tube furnace at 3100 K; they found a broad unresolved feature at $\sim$2000 cm^{-1} which is $\sim$370 cm^{-1} wide and unambiguously identified with the asymmetric stretch ro-vibrational band of C_3.

Gautschy-Loidl et al. (2004) compared phase-dependent observed and synthetic carbon star spectra, the calculations being based on dynamical model stellar atmospheres by Höfner et al. (2003). Of specific interest was the comparison with the C_3 $\sim$5 μm feature which Gautschy-Loidl et al. (2004) had difficulty in modelling. Among possible explanations in need of investigation is Höfner et al.'s (2003) use of opacities from the Jørgensen (1997) data base which in the C_3 case are based on the line list by Jørgensen, Almlöf & Siegbahn (1989). Tennyson & Yurchenko (2018) present an ExoMol (Tennyson & Yurchenko 2012) atlas of molecular opacities and note that by modern standards the Jørgensen et al. (1989) C_3 line list cannot be considered reliable, given improved methods and routine tuning of calculated line frequencies to experimental data.

Rocha & Varandas (2015) published a global *ab initio* potential energy surface (PES) obtained using calculations at the multi-reference configuration interaction (MRCI) and full-valence complete active space (FVCAS) with a triple-ζ augmented correlation consistent basis set (AVTZ) level of theory, which correctly describes the overall topology of the C_3 electronic ground state; this includes the all important conical intersections.Quite good agreement is achieved for pure bending modes but the stretching modes are not calculated with the accuracy required for a high quality line list. However, Schröder & Sebald (2016) calculated an accurate local (near equilibrium) *ab initio* PES using the fc-CCSD(T∗)-F12b/aug-cc-pV5Z level of theory which reproduces all then available rotational–vibrational term energies to better than 1 cm^{-1}; they achieve this by taking special care with potential energy convergence relative to high-order correlation effects, core–variance correlation, basis set size, and scalar relativity. Moreover, the rotational constants exhibit relative errors of not more than 0.01 per cent. Regardless of a decent *ab initio* quality, this is still not sufficiently accurate for line list applications. We have therefore constructed a new PES for C_3 by refining an *ab initio* PES to experimentally derived ro-vibrational energies by Tennyson (2024) and chosen the Schröder & Sebald (2016) PES as a starting point for these refinements.

Schröder & Sebald (2016) reported an *ab initio* electric dipole moment surface (EDMF) of C_3 using the fc-CCSD(T∗)-F12b/AV5Z level of theory which we adopt in our line list intensity calculations. Note that this allows us to provide absolute transition intensities for all transitions that we consider, something missing from all experimental studies reported up until now.

Tennyson et al. (2024b) summarized progress made with the ExoMol project up to April 2024, and the provision of a data base from which line lists and associated data may be retrieved. Examples of available line lists include alkali metal hydroxides (KOH and NaOH; Owens, Tennyson & Yurchenko 2021), silicon monoxide (Yurchenko et al. 2022), calcium and magnesium monohydride (CaH and MgH; Owens et al. 2022a), silicon mononitrate (SiN; Semenov et al. 2022), calcium monohydroxide (CaOH; Owens et al. 2022b), H_3^+ isotopologues (H_3^+, H_2D^+, HD_2^+, and D_3^+; Bowesman et al. 2023), thioformaldehyde (Mellor et al. 2023), aluminium monochloride (AlCl; Yurchenko et al. 2023), lithium hydroxide (LiOH; Owens et al. 2024a), yttrium oxide (YO; Yurchenko et al. 2024b), sulphur monoxide (SO; Brady et al. 2024), aluminium hydride and aluminium deuteride (AlH and AlD; Yurchenko et al. 2024c), and the methylidene cation (CH^+; Pearce, Yurchenko & Tennyson 2024).

Reported in this paper are calculations which produce ExoMol data base line lists for $^{12}C_3$, $^{12}C^{13}C^{12}C$, and $^{12}C^{12}C^{13}C$; the choice of isotopologues having been influenced by the detection by Giesen et al. (2020) of $^{12}C^{13}C^{12}C$ and $^{12}C^{12}C^{13}C$ in the direction of Sgr B2(M). Breier et al. (2016) mention an earlier failure to find interstellar $^{12}C^{12}C^{13}C$ using the *Herschel* space telescope, assuming a ν_2 lowest bending mode of 60.747 cm^{-1} for $^{12}C^{12}C^{13}C$ as Krieg et al. (2013) reported. Laboratory experiments by Breier et al. (2016) identified the $\nu_2 = 60.747$ cm^{-1} absorption as belong to $^{13}C^{13}C^{12}C$; as this was not observed, we concluded that there was no immediate need for isotopolgue line lists where more than one ^{12}C has been substituted by ^{13}C.

The summary of early work on C_3 presented above is necessarily brief and focussed on astronomical spectroscopy. For more details, including laboratory studies, see Martin-Drumel et al. (2023) and Tennyson (2024).

2 RO-VIBRATIONAL CALCULATIONS

Yurchenko, Thiel & Jensen (2007) published the variational methodology and associated programme TROVE (Theoretical ROVibrational Energies) for general calculations of ro-vibrational energies for an arbitrary small or medium-sized polyatomic. For triatomics, TROVE can use an exact kinetic energy operator (KEO) as developed by Yurchenko & Mellor (2020) for quasi-linear molecules, adopted here for our C_3 line list calculations using the PES and EDMF discussed below. We follow closely the calculation procedure described in detail by Yurchenko et al. (2020), where TROVE was used to compute a ro-vibrational line list for CO_2. The KEO is built using the bisector frame and valence coordinates r_1, r_2 (bond lengths), and $\rho = \pi - \alpha$, where α is a bond angle.

TROVE uses numerically constructed 1D primitive basis functions optimized for a given PES. The stretching basis functions $\phi_{n_1}(r_1)$ and $\phi_{n_2}(r_2)$ are generated using a Numerov–Cooley procedure (Noumerov 1924; Cooley 1961), while the bending basis functions $\phi_{n_3}(\rho)$ are obtained by solving the corresponding Schrödinger equation using associated Laguerre polynomials, see Yurchenko & Mellor (2020). For C_3, the basis set was limited by the following conditions :

$$n_1 + n_2 + n_3 \leq 56, \tag{1}$$

and $n_1 \leq 30$, $n_2 \leq 30$, and $n_3 \leq 56$, where n_3 is the bending vibrational quantum number used by TROVE. Extra bending functions are needed to allow for the low frequency of the bending mode and the large range of angles (approaching 90°) sampled by the excited bending states we consider here. The primitive basis functions are then further improved through a two-step contraction procedure. The final ro-vibrational basis functions are formed as symmetrically adapted products [see Yurchenko, Yachmenev & Ovsyannikov (2017) for details]

$$\Phi_{n,K}^{J,\Gamma} = \Phi_n^{(J=0),\Gamma_{\rm vib}} |J, K, \tau\rangle, \tag{2}$$

where $\Phi_n^{(J=0),\Gamma_{\rm vib}}$ is an eigenfunction of the vibrational ($J = 0$) Schrödinger equation and $|J, K, \tau\rangle$ is a symmetry adapted (Wang) rigid rotor wavefunction, τ is its parity, $K = |k|$ with k as a projection of the rotational angular momentum on the molecular axis z and n is a generalized vibrational index $n = (n_1, n_2, n_3)$. In equation (2), Γ and

Table 1. Comparison between calculated (TROVE) and observed (MARVEL) state energies used in potential energy surface fitting.

v_1	v_2	l_2	v_3	J	p	State energy (cm^{-1})		
						TROVE	MARVEL	O − C
0	0	0	0	0	e	0.000000	0.0	0.00000
0	1	1	0	1	e	63.853305	63.8533045(4)	−0.00000
0	2	0	0	0	e	132.795482	132.795(6)	−0.00048
0	2	2	0	2	e	133.938774	133.939(6)	+0.00023
0	3	1	0	1	e	207.872923	207.873(6)	+0.00008
0	4	0	0	0	e	286.557525	286.558(6)	+0.00047
0	4	2	0	2	e	288.155899	288.156(6)	+0.00010
0	4	4	0	4	e	291.042029	291.042(16)	−0.00003
0	5	3	0	3	e	373.462909	373.463(5)	+0.00009
0	5	5	0	5	e	377.523167	377.523(5)	−0.00017
1	0	0	0	0	e	1224.524735	1224.52(1)	−0.00473
0	1	1	1	1	f	2078.957902	2078.957(3)	−0.00090
0	2	2	1	2	f	2128.302969	2128.302(8)	−0.00097
0	4	4	1	4	f	2251.089429	2251.089(15)	−0.00043
0	5	5	1	5	f	2322.740567	2322.741(7)	+0.00043
0	5	3	1	3	f	2329.286309	2329.286(9)	−0.00031
2	0	0	0	0	e	2436.126153	2436.1(6)	−0.02615
1	1	1	1	1	f	3330.949595	3330.9496(5)	+0.00000
1	0	0	2	0	e	5268.399364	5268.399(2)	−0.00036
2	0	0	2	0	e	6460.662620	6460.663(2)	+0.00038
3	0	0	2	0	e	7635.526541	7635.526(18)	−0.00054
4	0	0	2	0	e	8799.534353	8799.5(6)	−0.03435

Γ_{vib} are the total and vibrational basis symmetries, respectively. For the two symmetric isotopologues $^{12}C_3$ and $^{12}C^{13}C^{12}C$, the C_{2v}(M) molecular symmetry group (Bunker & Jensen 1998) is used to classify the ro-vibrational eigen-solutions spanning four irreducible representations A_1, A_2, B_1, and B_2. For the asymmetric isotopologue $^{12}C^{12}C^{13}C$, the C_s(M) molecular symmetry group is used for the final ro-vibrational states. Internally, we employed the so-called artificial extended molecular symmetry group C_{Nv} (AEM) (Mellor, Yurchenko & Jensen 2021; Yurchenko, Mellor & Tennyson 2024d) to classify the rotational and bending basis functions, which helped reduce the memory requirement. Here,N corresponds to the maximal value of the rotational quantum number K, $K_{max} = 10$.

3 POTENTIAL ENERGY AND DIPOLE MOMENT SURFACES

Tennyson (2024) extracted observed transition wavenumbers within and between the $\tilde{X}\,^1\Sigma_g{}^+$ and $\tilde{A}\,^1\Pi_u C_3$ states from 21 publications, subjecting these to a Measured Active Rotational-Vibrational Energy Levels (MARVEL; Furtenbacher, Császár & Tennyson 2007; Tennyson et al. 2024a) analysis which yields 1887 empirical energy levels. We refined the Schröder & Sebald (2016) PES using those $\tilde{X}\,^1\Sigma_g{}^+$ corrected energy levels Tennyson (2024) lists in his table 3, with the exception of those at 4081.9, 4199.9, 4333.9, and 4486.7 cm^{-1} for which the energy uncertainties were comparatively high at 0.5 cm^{-1}.

PES refinement followed the procedure described in detail by Yurchenko (2023) and used for many ExoMol line list calculations, including the very recent works on H_2CS (Mellor et al. 2023), CH_4 (Yurchenko et al. 2024a), OCS (Owens et al. 2024b), and N_2O (Yurchenko et al. 2024d). The equilibrium bond length and angle adopted were those Schröder & Sebald (2016) use. Following Yurchenko (2023), our refined PES was also constrained to the Schröder & Sebald PES at geometries not represented by MARVEL corrected state energies used in the PES refinement. For the refinements, we selected 276 ro-vibrational MARVEL term values for J = 0–10, 20, 30, 40, 50, and 60 with low uncertainties (< 0.1 cm^{-1}). These were reproduced with a root mean square (rms) of 0.026 cm^{-1}.

The quality of the fit is illustrated in Table 1, where we show TROVE predictions for 21 states compared to MARVEL energy levels for the $\tilde{X}\,^1\Sigma_g{}^+C_3$ state (Tennyson 2024, his table 3). Tennyson's assignments are also replicated in Table 1: v_1 – symmetric stretch, v_2 – bend, l_2 – projection of J on to the bond angle bisector, v_3 – asymmetric stretch, J – rotational quantum number, and p – rotationless parity (e even or f odd). Here,v_1, v_2, l_2 and $v_3$are spectroscopic (normal mode) quantum numbers, which can be correlated to the TROVE quantum numbers n_1^T, n_2^T, n_3^T as given by

$$v_1 + v_3 = n_1^T + n_2^T,$$
$$v_2 = 2n_3^T + l_2.$$

In Table1, MARVEL energy uncertainties were placed in parentheses and give Tennyson's estimate of the error in the least significant digits provided. TROVE and MARVEL state energies were in agreement, even at ∼8800 cm^{-1} to within experimental error in the latter; this was unexpected given the presence of conical intersections to be discussed below. Table 1 residuals have a mean of $-(3.2 \pm 9.1) \times 10^{-3} cm^{-1}$.

Schröder & Sebald (2016) construct their EDMF from 372 symmetry-unique nuclear configurations. Local transformation to the Eckart coordinate system yields parallel and perpendicular components. Least squares fits gave Schröder & Sebald analytical expressions for the two components which we adopted for our line list calculations.

To summarize, our spectroscopic model consists of a refined PES and an *ab initio* DMS of C_3, in its ground electronic state. We do not take into account any conical intersections or other couplings with other electronic states, see, e.g. Rocha & Varandas (2015), nor any pre-dissociative effects – C_3 has a high dissociation energy, ∼ 6.3 eV (Rocha & Varandas 2015).

4 LINE LIST CALCULATIONS

Table 2 lists TROVE input parameters selected, as well as numbers of states and transitions calculated in each case. Adopted carbon atom masses were 11.996709 and 13.00006335 Da; these are nuclear masses, with core valence electron masses added. Transitions included in our line lists were limited to those for which the upper state energy is less than 20 000 cm^{-1} and the lower state energy is less than 10 000 cm^{-1}. A lower state energy maximum of 10 000 cm^{-1} was selected in order to provide the sufficient temperature coverage for $^{12}C^{12}C^{13}C$ absorption spectra simulations, while the upper energy thresholds is to maintain the line list completeness for the wavenumber range of 0–10 000 cm^{-1}. Rotation quantum number J upper limits were matched to the lower state energy threshold, above which no further population of ro-vibrational states were considered.

State energies in $^{12}C^{13}C^{12}C$ are slightly lower than corresponding state energies in $^{12}C_3$, resulting in more being selected below a given maximum state energy, leading to more transitions being calculated in the $^{12}C^{13}C^{12}C$ case. A much larger number of transitions calculated for the $^{12}C^{12}C^{13}C$ isotopologue is a consequence of more parity-allowed transitions in the case of an asymmetric molecule. Indeed, only even-parity states (A_1 and A_2) exist for $^{12}C_3$ and $^{12}C^{13}C^{12}C$ due to zero nuclear spin of ^{12}C and the Pauli principle, while the asymmetric species $^{12}C^{12}C^{13}C$ has no such restrictions and all states are present.

The line lists are provided in the ExoMol format (Tennyson et al. 2024b), which consists of a two file-type set, a states file and transitions files, augmented by a partition function. The states file for C_3 contains the ro-vibrational energy term values, quantum numbers,

Table 2. TROVE input parameters and numbers of transitions calculated.

Isotopologue	Number of basis functions	Energy maximum (cm^{-1})	J range	l_2 range	Number of states	Number of transitions
$^{12}C_3$	56	20000	0 – 155	0 – 12	2166503	5481690507
$^{12}C^{13}C^{12}C$	56	20000	0 – 155	0 – 12	2282841	6071530477
$^{12}C^{12}C^{13}C$	45	17000	0 – 150	0 – 10	2442205	14503868150

Table 3. Extract from the `.states` file of the 'AtLast' C_3 line list.

i	$\tilde{E}$ (cm^{-1})	g	J	unc. (cm^{-1})	τ (s^{-1})	Γ_{tot}	v_1	v_2	l_2	v_3	Γ_{vib}	C_i	n_1^T	n_2^T	n_3^T	Ca/Ma	$\tilde{E}_T$ (cm^{-1})
39668	18.082083	13	6	0.000234	NaN	A1	0	0	0	0	A1	1.0000	0	0	0	Ma	18.082390
39669	150.215573	13	6	0.005745	5.8667E+01	A1	0	2	2	0	A1	0.9900	0	0	0	Ma	150.216293
39670	151.792684	13	6	0.001821	7.0628E+01	A1	0	2	0	0	A1	−0.9900	0	0	1	Ma	151.801811
39671	301.417834	13	6	0.009863	2.4206E+01	A1	0	4	4	0	A1	−1.0000	0	0	0	Ma	301.414477
39672	304.941414	13	6	0.005745	2.8200E+01	A1	0	4	2	1	A1	−0.9600	0	0	1	Ma	304.932485
39673	306.313661	13	6	0.005745	3.0356E+01	A1	0	4	0	2	A1	−0.9600	0	0	2	Ma	306.289813
39674	468.895204	13	6	0.064200	1.3788E+01	A1	0	6	6	0	A1	1.0000	0	0	0	Ca	468.895204
39675	474.279718	13	6	0.064200	1.5230E+01	A1	0	6	4	1	A1	−1.0000	0	0	1	Ca	474.279718
39676	477.142161	13	6	0.064200	1.6970E+01	A1	0	6	2	2	A1	0.9200	0	0	2	Ca	477.142161

Notes.i: state counting number. $\tilde{E}$: state energy in cm^{-1}. g_{tot} : total state degeneracy. J: total angular momentum. unc.: uncertainty cm^{-1}. τ: life time in s. Γ: total symmetry index in C_{2v}(M). v_1: symmetric stretching normal mode quantum number. v_2: normal mode bending quantum number. l_2: normal mode vibrational angular momentum quantum number. v_3: asymmetric stretching normal mode quantum number.Γ_{vib}: vibrational symmetry index in C_{2v}(M). C_i: coefficient with the largest contribution to the ($J = 0$) contracted set; $C_i \equiv 1$ for $J = 0$. n_1^T: TROVE stretching vibrational quantum number. n_2^T: TROVE stretching vibrational quantum number. n_3^T: TROVE bending vibrational quantum number. Label: '`Ma`' for MARVEL, '`Ca`' for calculated. Calc: original TROVE calculated state energy (in cm^{-1}).

Table 4. Extract from the transitions file for the 'AtLast' line list for C_3.

f	i	A_{fi}
286793	299447	2.6382e-16
1115453	1124869	5.5991e-16
1144929	1134888	7.8148e-16
1200446	1172433	1.2177e-15
1329282	1320088	2.4308e-16
879962	869764	2.4688e-16
1464383	1455885	7.3244e-16
616080	582311	1.8432e-15
442578	430254	2.8786e-16

Notes.f: upper state counting number. i: lower state counting number. A_{fi}: Einstein A-coefficient in s^{-1}.

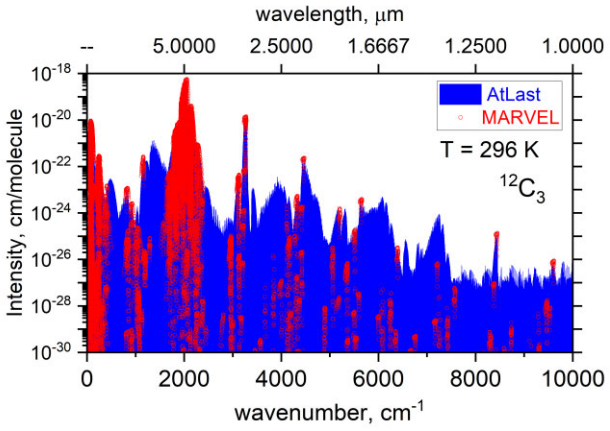

Figure 1. A room temperature ($T = 296$ K) 'stick spectrum' generated using ExoCross (Yurchenko, Al-Refaie & Tennyson 2018) of $^{12}C_3$ computed using the 'AtLast' line list, with the height of the sticks representing the transition line intensity (absorption coefficient) and their position representing the corresponding transition wavenumber. The MARVELized transitions are indicated using circles.

life times, uncertainties, and state degeneracies. Each state is labelled with a state ID, a counting number. The structure of the C_3 states file is illustrated in Table 3 where we show an extract from the 'AtLast' line list for $^{12}C_3$. We note that while the quantum number labels given for levels labelled 'Ma' for MARVELized can be regarded as secure; the quantum labels for other levels are automatically generated by TROVE and represent only best estimates.

Transitions files contain Einstein A-coefficients and upper/lower state IDs and divided into 10 files in 1000 cm^{-1} ranges. An extract from a $^{12}C_3$ transition file is given in Table 4. We used the $^{12}C_3$ MARVEL energies of Tennyson (2024) to replace the calculated values where available. These entries are indicated in the states file with the label 'Ma'. The coverage of the MARVELized data is illustrated in Fig. 1, where we show a room temperature ($T = 296$ K) spectrum of $^{12}C_3$ and the MARVELized lines indicated with the red circles. At this temperature, there are 16 178 MARVELized transitions which provide the experimental accuracy as based on the experimental uncertainties of the MARVEL data set by Tennyson (2024). These high-accuracy transitions can be accessed via the new ExoMolHR web app (Zhang et al. 2024).

5 CROSS-SECTION, PARTITION FUNCTION, AND OPACITY ESTIMATES

Yurchenko et al. (2018) provided a general utility programme (ExoCross) for processing transition and states files generated by TROVE and other programmes. ExoCross was used to calculate cross-sections and partition functions based on transitions and

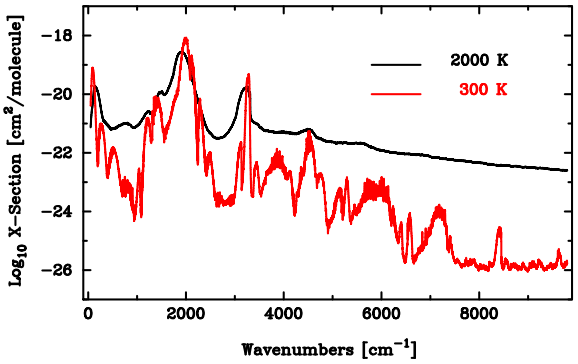

Figure 2. Computed cross-sections for the $\tilde{X}\,^1\Sigma_g^+$ electronic ground state of $^{12}C_3$ at 300 and 2000 K.

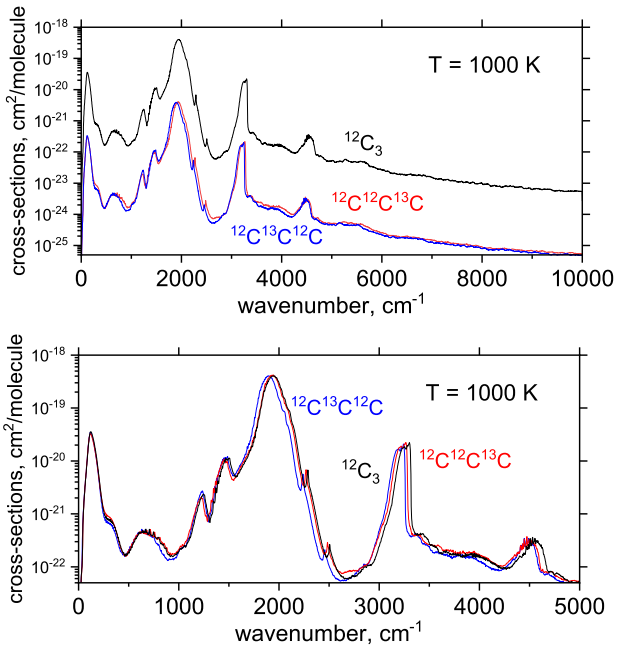

Figure 3. Computed cross-sections for the $\tilde{X}\,^1\Sigma_g^+$ electronic ground state of $^{12}C_3$, $^{12}C^{13}C^{12}C$, and $^{12}C^{12}C^{13}C$ at 1000 K: scaled by their natural abundances (top display) to show their relative importance and not-scaled (bottom display) to show their relative displacements.

corresponding ro-vibrational states calculated with TROVE for the $\tilde{X}\,^1\Sigma_g^+$ electronic ground state of C_3.

Fig. 2 shows derived cross-sections, at 300 K (red curve) and 2000 K (black curve), for the $^{12}C_3$ electronic ground state sampled at 1 cm^{-1} intervals and convolved with a Gaussian of half width at half-maximum (HWHM) of 1 cm^{-1}. Of particular note is the peak near 2000 cm^{-1}which was understood to correspond with the laboratory measurement by Treffers & Gilra (1975, their figure 2). The weaker band at 3300 cm^{-1} can also be identified.

Cross-sections for all three isotopologues were similarly calculated for electronic ground states at 1000 K, sampled at 1 cm^{-1} intervals and convolved with Gaussians of HWHM = 1 cm^{-1} and plotted in Fig. 3. The top display, where cross-sections are scaled by relative $^{12}C_3$ and $^{13}C_3$ solar abundances, illustrates the relative importance of different isotopologues of C_3, while the bottom display, where the unscaled cross-sections are overlaid, illustrates the isotope frequency shift between $^{12}C_3$, $^{12}C^{13}C^{12}C$, and $^{12}C^{12}C^{13}C$,

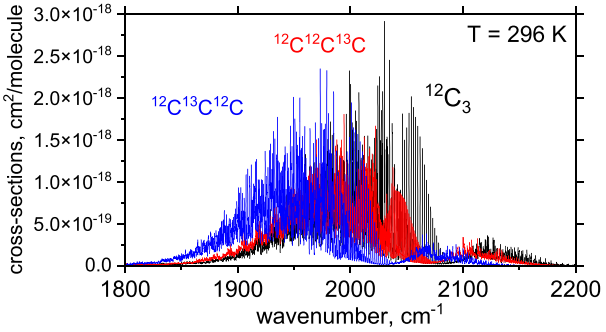

Figure 4. Computed cross-sections for $^{12}C_3$, $^{12}C^{12}C^{13}C$, and $^{12}C^{13}C^{12}C$ 2000 cm^{-1} bands at a temperature of 296 K shown as 'stick-spectra'.

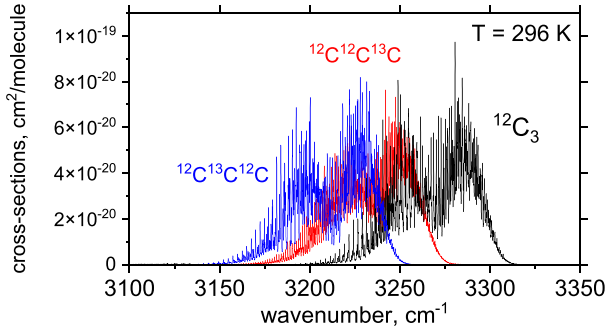

Figure 5. Computed cross-sections for $^{12}C_3$, $^{12}C^{12}C^{13}C$ and $^{12}C^{13}C^{12}C$ 3300 cm^{-1} bands at a temperature of 296 K shown as 'stick-spectra'.

which is discernable and can be seen even at low resolution in Fig. 3. The consequences for the computed transition frequencies when a ^{13}C replaces a ^{12}C atom were more obvious in Figs 4 and 5 where the 2040 and 3300 cm^{-1} bands for all three isotopologues are plotted, showing differences of about 50 cm^{-1}.

Temperature-dependent partition functions were obtained as Boltzmann sums over all states in a line list:

$$Q(T) = \sum_i g_i^{(\mathrm{ns})}(2J_i + 1)e^{-c_2\tilde{E}_i/T},$$

where $\tilde{E}_i$ is the energy term value for state i (cm^{-1}) calculated with TROVE for the $\tilde{X}\,^1\Sigma_g^+$ electronic ground state of C_3, J_i is the corresponding total angular momentum, k is the second radiation constant (cm K^{-1}), $g_i^{(\mathrm{ns})}$ is the state dependent nuclear spin degeneracy, and T is the temperature (K). Since our partition functions only include states from the ground electronic states and therefore are not complete, especially at high temperatures, they thus represent lower limits.

Note that ExoMol uses the HITRAN convention for partition functions which include the full nuclear spin degeneracy. Since ^{12}C has zero nuclear spin, there is no difference for $^{12}C_3$, but for the ^{13}C-containing isotopologues considered here, our partition functions will be a factor of 2 larger than standard astrophysical ones which neglect the nuclear spin factor. The partition functions $Q(T)$ for $^{12}C_3$, $^{12}C^{13}C^{12}C$, and $^{12}C^{12}C^{13}C$ were computed using temperatures in the range 1 to 5000 K in 1 K steps using ExoCross, which calculates a finite sum over all calculated states following (for example) the approach which Neale & Tennyson (1995) adopt. The resulting dependence of partition function with temperature was plotted in Fig. 6. Given energy maxima and the J-range selected (Table 2),

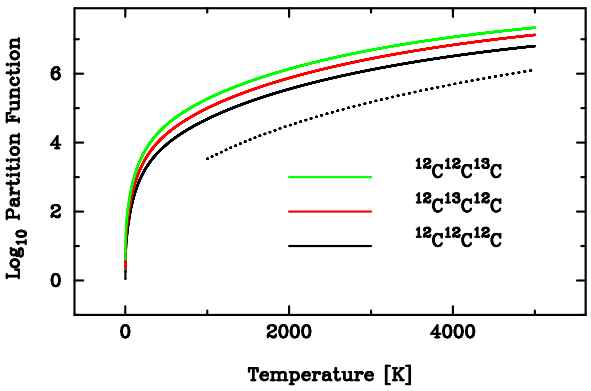

Figure 6. Isotopologue partition function comparisons with a C_3 estimate (dotted line) based on Irwin's (1981) polynomial coefficients.

partition functions plotted in Fig. 6 were fully converged. Irwin's (1981) polynomial coefficients lead to a $^{12}C_3$ partition function lower than our estimate by roughly one order of magnitude; this was anticipated as his polynomial coefficients are based on studies by Pitzer & Clementi (1959) and McBride et al. (1963), pre-dating pioneering work by Gausset et al. (1965) who demonstrated the importance of the contribution from the low frequency bending mode.

Apart from the states, transition, and partition function files, ExoMol line list compilations contain opacities and line-broadening parameters. Opacities in the form of cross-sections and k-tables (Lacis & Oinas 1991) were calculated following the procedure Chubb et al. (2021) describe, adopting their temperature and pressure grid. Molecular opacities for C_3 are provided in four files, each formatted for the exoplanet atmospheric retrieval code identified in the file name: ARCiS (Min et al. 2020), TauREx (Al-Refaie et al. 2021), NEMESIS (Irwin et al. 2008), and petitRADTRANS (Molliére et al. 2019).

As Blackwell, Booth & Petford (1984, their fig. 1) show, an accurate determination of the microturbulent velocity is required for a solar abundance determination based on several absorption lines, using precision oscillator strengths and a 1D static model stellar atmosphere in which radiation transfer occurs only along an observer's line of sight. Asplund et al. (2000) use more realistic dynamical model atmospheres, in which 3D radiation transfer is coupled with the convective velocity field; they show that a microturbulent velocity is an artefact of the static 1D model approximation and not needed. Retrieval codes for which we have provided C_3 opacities make no use of microturbulent velocity and we have accordingly ignored it in our opacity table calculations.

6 COMPARISON WITH EXPERIMENT

Martin-Drumel et al. (2023, their figure 5) present a Fourier transform infrared spectrum of C_3 in absorption from 1900 to 2100 cm^{-1}, deducing a 700 K rotational temperature and a Gaussian line-shape of width 0.005 cm^{-1} as their experimental conditions. Computed C_3 transitions and state energies were used with ExoCross to synthesise the Martin-Drumel et al. (2023) spectrum, assuming the same temperature and Gaussian width. The comparison is shown in Fig. 7: black is used for the Martin-Drumel et al. (2023) spectrum and red for the spectrum synthesized using C_3 transitions and energies reported in this paper. The wavenumber range plotted in Fig. 7 corresponds to the $\nu_3 \simeq 2000$ cm^{-1} broad absorption feature plotted in Figs 2 and 3.

A high-resolution inspection of individual lines plotted in Fig. 7 showed a maximum difference between observed and calculated line-positions of 0.03 cm^{-1}, as expected given the formal least-squares errors obtained using MARVEL energies for PES refinement described above. In most cases, calculated and observed line-positions agreed to better than 0.01 cm^{-1} as indicated by the state energy comparison presented in Table 1. Our calculated line-intensities are also in good agreement with the observed relative values, as may be seen in Fig. 7, showing the band structure to have been correctly calculated. Our values can be used to place observations on an absolute scale.

Best-fitting molecular vibrational term values (band centres) by Krieg et al. (2013, their tables 3, 5, and 7) for $^{12}C_3$, $^{12}C^{13}C^{12}C$, and $^{12}C^{12}C^{13}C$ are listed in Table 5 (Column 3) for comparison with our ($J = 0$) energies of C_3. The $^{12}C_3(0, 1^1, 0)$ energy term value in Column 4 was taken from Gendriesch et al. (2003, their table 2) and the $^{12}C^{12}C^{13}C(0, 0^0, 1)$ value in the same column was a refit to the measurements of Moazzen-Ahmadi & McKellar (1993) by Krieg et al. (2013, their table 7). With the exception of the $^{12}C_3(1, 0^0, 1)$ entry where the difference was larger than 0.8 cm^{-1}, satisfactory agreement is obtained. This is especially reassuring considering that our model (PES) was optimized for the main isotopologue only.

Breier et al. (2016, their table 3) use a terahertz-supersonic jet spectrometer, in combination with a laser ablation source, to measure ν_2 lowest bending mode transition frequencies of linear C_3 and its ^{13}C-substituted isotopologues. Table 6 compares the ν_2 lowest order bending mode transition frequencies for $^{12}C_3$, $^{12}C^{13}C^{12}C$, and $^{12}C^{12}C^{13}C$ extracted from our line lists with the Breier et al. (2016) measurements. In the $^{12}C_3$ case, calculated frequencies agree with experiment to 0.0005 cm^{-1} in the worst case ($J = 16$, R-branch); this was understood to be a consequence of MARVEL corrections having been applied and PES improvements that these made possible. The $^{12}C_3(1, 0^0, 1)$ frequency Krieg et al. (2013) deduce by fitting molecular parameters was noted above as differing from our states file entry by more than 0.8 cm^{-1}; this was reduced to 0.0005 cm^{-1} when the Breier et al. (2016, their table 3) measurement was adopted, as shown in Table 6.

Line lists for $^{12}C^{13}C^{12}C$ and $^{12}C^{12}C^{13}C$ have been prepared without MARVEL corrections as, to the best of our knowledge, necessary experimental data do not currently exist. As a result, the Table 6 comparison with experiment for ^{13}C-substituted isotopologues was less satisfactory. We also noted that use of a PES refined for $^{12}C_3$ would have been non-optimum for $^{12}C^{13}C^{12}C$ and $^{12}C^{12}C^{13}C$ line list calculations. While ν_2 lowest bending mode transition frequency residuals for $^{12}C^{13}C^{12}C$ were found to be always less than 0.03 cm^{-1} they are all positive and therefore indicative of an underlying systematic error.

Krieg et al. (2013) conduct infrared ($\sim$3 μm) high-resolution spectroscopy of C_3, also using a supersonic jet and a laser ablation source, in combination with a continuous-wave parametric oscillator as a radiation source. In Table 7, we compare our wavenumbers for (101) $\leftarrow$ (000) transitions with those Krieg et al. (2013, their tables 1, 4, and 6) measure. In the $^{12}C_3$ case, calculated frequencies agree with experiment to 0.0018 cm^{-1} in the worst case ($J = 22$, R-branch); this was again understood to be a consequence of MARVEL corrections having been applied and PES improvements that these made possible.

As with the Breier et al. (2016) comparison, the Table 7 comparison with experiment for ^{13}C-substituted isotopologues was less satisfactory. The absence of negative residuals is again apparent and indicative of an underlying systematic error in our $^{12}C^{13}C^{12}C$ and $^{12}C^{12}C^{13}C$ calculations. Identifying the origin of the apparent systematic error in our $^{12}C^{13}C^{12}C$ and $^{12}C^{12}C^{13}C$ line list calculations

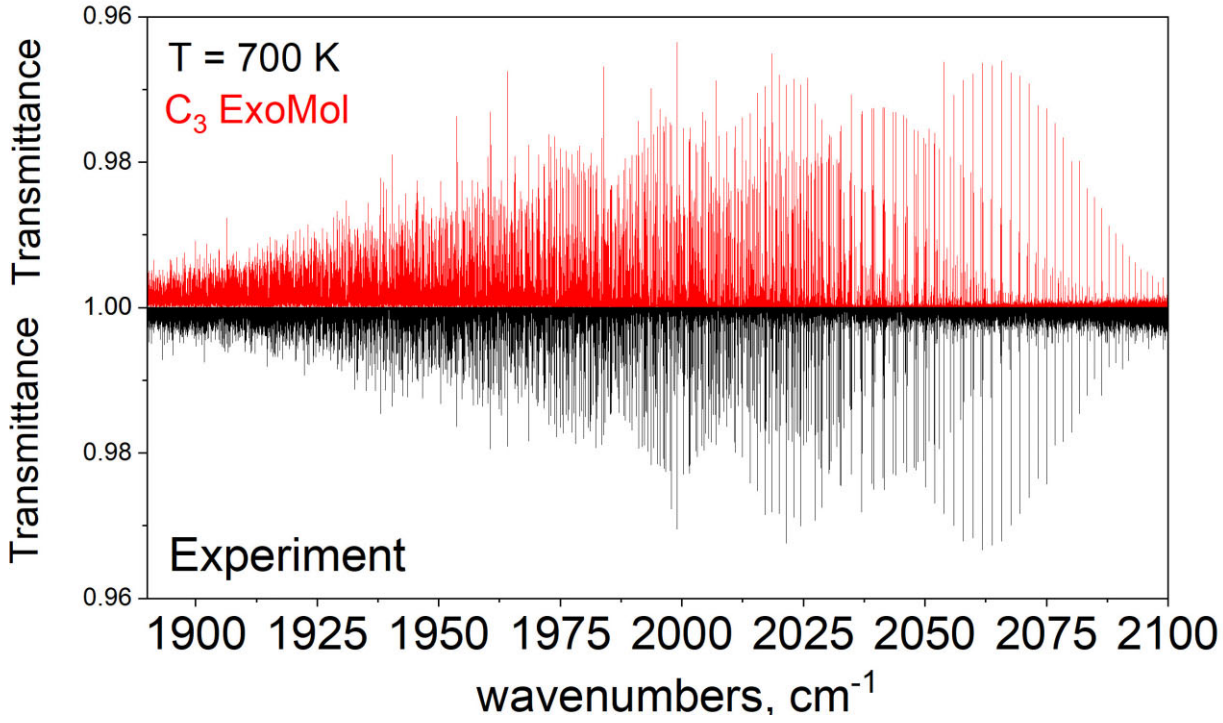

Figure 7. C_3 experimental spectrum due to Martin-Drumel et al. (2023) with the transmittance compared to the transmittance computed (see the text) for their experimental conditions using our $^{12}C_3$ line list and plotted in the lower panel. The irregular spikes in both spectra correspond to local accidental coincidences of line positions. These responses are very sensitive to the accuracy of calculations as well as experimental resolutions and are very difficult to reproduce, which explains their appearance at different places.

Table 5. Comparisons of theoretical vibrational term values of C_3 isotopologues with experimentally derived values from the literature.

Isotopologue	Vibrational state	Krieg et al. (cm^{-1})	Other (cm^{-1})	TROVE (cm^{-1})
$^{12}C_3$	$(0, 1^1, 0)$	63.4165946	63.4165889	63.415212
	$(0, 0^0, 1)$	2040.019278		2040.017256
	$(0, 1^1, 1)$	2078.500541		2078.48975
	$(1, 0^0, 1)$	3260.127048		3260.974851
	$(1, 1^1, 1)$	3330.508589		3330.503579
$^{12}C^{12}C^{13}C$	$(0, 0^0, 1)$	2027.20779	2027.2078	2027.201829
	$(1, 0^0, 1)$	3224.7509		3224.733608
$^{12}C^{13}C^{12}C$	$(1, 0^0, 1)$	3205.59319		3205.561181

was regarded as beyond the scope of this study but an obvious first step would be to test the validity of the PES used, especially as this had been carefully refined to optimise $^{12}C_3$ calculations.

7 DISCUSSION

Treffers & Gilra (1975) showed experimentally that the $\upsilon_3 \simeq 2000$ cm^{-1} broad absorption feature completely dominates the integrated C_3 cross-section at 3100 K, with transitions calculated in this paper showing that this extends downwards to temperatures of 300 K. The $\upsilon_3 \simeq 2000\,cm^{-1}$ band was therefore found to completely dominate the infrared C_3 opacity as Gilra (1973) suggests. As C_3 transitions computed in this paper reproduce the $\upsilon_3 \simeq 2000$ cm^{-1} band Martin-Drumel et al. (2023) observe, it was clear that our line lists could be used to calculate the C_3 contribution to molecular opacity at temperatures less than ∼5000 K; this limit is a consequence of the fact that our lower state energies were limited to states below 10 000 cm^{-1}.

Marigo et al. (2022) provide low-temperature gas opacities. In the C_3 case, Marigo et al. (2022) estimate this contribution using the line list by Jørgensen et al. (1989). Our $^{12}C_3$ line list is complete to transition frequencies of 10000 cm^{-1} or less and our associated states file complete for electronic ground state ro-vibrational energies less than 20 000 cm^{-1}; it is therefore an improvement on the earlier line list by Jørgensen et al. (1989), especially as our calculated stretching frequencies are in very much better agreement with experimental determinations. An immediate application of our line lists for C_3 and its ^{13}C-substituted isotopologues would be to update Marigo et al. (2022) low-temperature gas opacities. As part of this work, a similar update has been applied to the ExoMolOP data base (Chubb et al. 2021) which did not include a C_3 contribution.

Use of high-dispersion transit spectroscopy to detect and characterize extra-solar planets, by Guilluy et al. (2019) for example, requires line lists for individual molecules having accurate line-positions and relative intensities. Our $^{12}C_3$ line list was understood to be suitable for high-dispersion transit spectroscopy at wavelengths longer than ∼2.5 μm (∼ 4000 cm^{-1}). Making our $^{12}C_3$ line list suitable for high-dispersion transit spectroscopy at shorter wavelengths would be complicated by the presence of conical intersections as Yarkony (1996), Worth & Cederbaum (2004) and Schuurman & Stolow (2018) review. Briefly, in the Born–Oppenheimer approximation, nuclei move on potential energy surfaces corresponding to associated electronic states; these may intersect at a point in nuclear coordinates with the topology of a double cone. While Rocha & Varandas (2018) improve on the PES by Rocha & Varandas (2015) and achieve an accurate representation in the vicinity of the four conical

Table 6. Comparison of observed (Breier et al. 2016) and calculated $(0, 1^1, 0) - (0, 0^0, 0)$ transition frequencies.

Isotopologue	Branch	J	Observed (cm^{-1})	Calculated (cm^{-1})	O–C (cm^{-1})
$^{12}C_3$	P	2	61.2698	61.2698	−0.0000
		4	59.6376	59.6376	−0.0000
		6	58.0776	58.0775	0.0001
		8	56.5900	56.5900	0.0000
		10	55.1744	55.1744	0.0000
		12	53.8307	53.8307	0.0000
		14	52.5584	52.5582	0.0002
		16	51.3567	51.3566	0.0000
$^{12}C_3$	Q	2	63.0622	63.0622	0.0000
		4	63.2673	63.2673	0.0000
		6	63.5886	63.5886	−0.0000
		8	64.0247	64.0247	0.0000
		10	64.5737	64.5737	0.0000
		12	65.2334	65.2334	−0.0000
		14	66.0012	66.0012	0.0000
		16	66.8741	66.8741	−0.0000
$^{12}C_3$	R	0	63.8533	63.8533	−0.0000
		2	65.6653	65.6653	0.0000
		4	67.5485	67.5484	0.0000
		6	69.5023	69.5023	−0.0000
		8	71.5262	71.5262	−0.0000
		10	73.6193	73.6193	−0.0000
		12	75.7806	75.7806	−0.0001
		14	78.0089	78.0090	−0.0000
		16	80.3032	80.3027	0.0005
$^{12}C^{13}C^{12}C$	P	2	58.9045	58.8754	0.0291
		4	57.2690	57.2397	0.0293
		6	55.7018	55.6727	0.0291
		8	54.2020	54.1744	0.0276
		10	52.7683	52.7448	0.0235
		12	51.3987	51.3834	0.0153
$^{12}C^{13}C^{12}C$	Q	2	60.6952	60.6663	0.0289
		4	60.8970	60.8681	0.0290
		6	61.2132	61.1841	0.0291
		8	61.6423	61.6131	0.0292
		10	62.1824	62.1532	0.0293
		12	62.8312	62.8020	0.0292
$^{12}C^{13}C^{12}C$	R	0	61.4863	61.4573	0.0289
		2	63.2928	63.2638	0.0290
		4	65.1667	65.1380	0.0287
		6	67.1064	67.0792	0.0272
		8	69.1102	69.0870	0.0232
		10	71.1755	71.1603	0.0152
		12	73.2996	73.2986	0.0010
$^{12}C^{12}C^{13}C$	P	2	61.0766	61.0770	−0.0004
		3	60.2841	60.2845	−0.0003
		4	59.5091	59.5094	−0.0003
		5	58.7516	58.7518	−0.0001
		6	58.0117	58.0116	0.0001
		7	57.2893	57.2890	0.0003
		8	56.5844	56.5838	0.0007
		9	55.8971	55.8960	0.0011
		10	55.2274	55.2257	0.0017
		11	54.5751	54.5727	0.0024
		12	53.9403	53.9370	0.0034
$^{12}C^{12}C^{13}C$	Q	1	62.7421	62.7425	−0.0004
		2	62.7981	62.7984	−0.0004
		3	62.8819	62.8823	−0.0003
		4	62.9936	62.9939	−0.0003
		5	63.1331	63.1333	−0.0002
		6	63.3000	63.3001	−0.0001
		7	63.4944	63.4944	−0.0000
		8	63.7159	63.7159	0.0001
		9	63.9644	63.9643	0.0002
		10	64.2396	64.2394	0.0002
		11	64.5411	64.5410	0.0002
		12	64.8687	64.8687	0.0001
$^{12}C^{12}C^{13}C$	R	0	63.5590	63.5594	−0.0004
		1	64.4212	64.4216	−0.0004
		2	65.3008	65.3011	−0.0003
		3	66.1977	66.1978	−0.0001
		4	67.1118	67.1117	0.0001
		5	68.0431	68.0428	0.0004
		6	68.9916	68.9908	0.0008
		7	69.9571	69.9558	0.0013
		8	70.9396	70.9376	0.0020
		9	71.9390	71.9362	0.0028
		10	72.9553	72.9514	0.0039
		11	73.9882	73.9831	0.0052
		12	75.0379	75.0312	0.0067

intersections, they do not claim an improvement for other geometries. Further PES development work will therefore be needed.

As Hinkle, Keady & Bernath (1988) note, the 4050 Å line cannot be used to detect C_3 in the interstellar medium and cool stars through the lack of ultraviolet flux; they identify this molecule in the circumstellar shell surrounding the obscured carbon star IRC+10216 using observed line positions from which molecular constants were deduced. Detection of C_3, where it exits, is important as chemical models of the environment are then constrained and our $^{12}C_3$ line list should facilitate searches when infrared or radio data are available. A kinematic analysis using lines of molecular species, identified and for which number densities are known through a reliable chemical model, establishes star formation modes as Seo et al. (2019) demonstrate.

As it is understood from stellar evolution calculations (Sweigart, Greggio & Renzini 1989) that ^{13}C will be enriched in stars ascending the giant and asymptotic giant branches due to dredge-up, and Giesen et al. (2020) detect $^{12}C^{13}C^{12}C$ and $^{12}C^{12}C^{13}C$ in the interstellar medium towards Sgr B2(M), future work to improve our line lists for these isotopologues would seem to be worthwhile. More laboratory work to create experimental line lists for $^{12}C^{13}C^{12}C$ and $^{12}C^{12}C^{13}C$ would enable the MARVEL procedure to be applied; PES refinement should follow for both cases, allowing improved line lists to be calculated.

Lagarde et al. (2024) obtain $^{12}C_3/^{13}C_3$ abundance ratios for 71 field red giants and identify cases where $^{12}C_3/^{13}C_3 \leqslant 10$. The relative contribution to stellar interior opacity, and therefore to stellar structure, by isotopologues having one or more ^{12}C substituted by a ^{13}C atom, will become increasingly important as the $^{12}C_3/^{13}C_3$ ratio decreases. Additional line lists for the remaining isotopologues ($^{13}C^{12}C^{13}C$, $^{13}C^{13}C^{12}C$, and $^{13}C^{13}C^{13}C$) could be computed should the need arise.

8 CONCLUSIONS

We have calculated new 'AtLast' line lists for the electronic ground state of the C_3 molecule and its two ^{13}C-substituted isotopologues, known to be important in astrophysics. We have made the transition, states, and partition function files available through the ExoMol

Table 7. Comparison of observed (Krieg et al. 2013) and calculated $(1, 0^0, 1)$– $(0, 0^0, 0)$ transition frequencies.

Isotopologue	Branch	J	Observed (cm^{-1})	Calculated (cm^{-1})	O − C (cm^{-1})
$^{12}C_3$	P	2	3258.3915	3258.3914	+0.0001
		4	3256.6061	3256.6061	−0.0000
		6	3254.7701	3254.7704	−0.0003
		8	3252.8857	3252.8858	−0.0001
		10	3250.9513	3250.9514	−0.0001
		12	3248.9690	3248.9702	−0.0012
		14	3246.9399	3246.9396	+0.0003
		16	3244.8634	3244.8637	−0.0003
		18	3242.7418	3242.7419	−0.0001
		20	3240.5760	3240.5776	−0.0016
		22	3238.3673	3238.3673	−0.0000
		24	3236.1143	3236.1143	+0.0000
		26	3233.8189	3233.8189	+0.0000
$^{12}C_3$	R	0	3260.9744	3260.9749	−0.0005
		2	3262.6340	3262.6338	+0.0002
		4	3264.2415	3264.2414	+0.0001
		6	3265.7983	3265.7982	+0.0001
		8	3267.3032	3267.3032	−0.0000
		10	3268.7595	3268.7587	+0.0008
		12	3270.1620	3270.1620	−0.0000
		14	3271.5163	3271.5160	+0.0003
		16	3272.8208	3272.8207	+0.0001
		18	3274.0776	3274.0775	+0.0001
		20	3275.2857	3275.2851	+0.0006
		22	3276.4472	3276.4454	+0.0018
		24	3277.5579	3277.5569	+0.0010
		26	3278.6059	3278.6059	+0.0000
$^{12}C^{13}C^{12}C$	P	2	3203.8601	3203.8279	+0.0322
		4	3202.0786	3202.0467	+0.0319
		6	3200.2508	3200.2182	+0.0326
		8	3198.3737	3198.3429	+0.0308
		10	3196.4519	3196.4212	+0.0307
		12	3194.4845	3194.4541	+0.0304
	R	0	3206.4418	3206.4098	+0.0320
		2	3208.1020	3208.0709	+0.0311
		4	3209.7142	3209.6835	+0.0307
		6	3211.2776	3211.2477	+0.0299
		8	3212.7938	3212.7634	+0.0304
		10	3214.2615	3214.2310	+0.0305
		12	3215.6799	3215.6506	+0.0293
$^{12}C^{12}C^{13}C$	P	1	3223.9235	3223.9062	+0.0173
		2	3223.0837	3223.0665	+0.0172
		3	3222.2317	3222.2146	+0.0171
		4	3221.3654	3221.3506	+0.0148
		5	3220.4872	3220.4744	+0.0128
		6	3219.5997	3219.5863	+0.0134
		7	3218.7039	3218.6862	+0.0177
		8	3217.7917	3217.7742	+0.0175
		9	3216.8658	3216.8505	+0.0153
		10	3215.9316	3215.9150	+0.0166
		11	3214.9840	3214.9679	+0.0161
$^{12}C^{12}C^{13}C$	R	0	3225.5661	3225.5488	+0.0173
		1	3226.3700	3226.3517	+0.0183
		2	3227.1603	3227.1422	+0.0181
		3	3227.9361	3227.9205	+0.0156
		4	3228.7025	3228.6864	+0.0161
		5	3229.4566	3229.4400	+0.0166
		6	3230.1982	3230.1812	+0.0170
		7	3230.9261	3230.9102	+0.0159
		8	3231.6438	3231.6269	+0.0169
		9	3232.3485	3232.3314	+0.0171
		10	3233.0410	3233.0237	+0.0173
		11	3233.7216	3233.7039	+0.0177

data base. Our line lists are applicable to studies of the interstellar medium as well as cool star and planetary atmospheres. In the $^{12}C_3$ case, the MARVEL procedure has provided experimental accuracy in all comparisons; the other two line lists are not as accurate, and improvements to be made in the future have been identified.

SUPPORTING INFORMATION

Supplementary data are available at *MNRAS* online.

Schröder & Sebald (2016)'s PES has been refined using experimental energy levels through the MARVEL procedure. Schröder & Sebald (2016, their table 3) provide non-redundant parameters which, when used with their equation 3.1, defines the PES they publish. Lines 4 – 61 of the file

`C3_pes_refined.inp`list our revisions to their non-redundant parameters; in the preceding lines, the number of data records, equilibrium bond-lengths in Å, and the equilibrium bond-angle supplement in degrees, have been provided. With the additional file

`C3_pes.f90`we have presented a FORTRAN90 programme which may be compiled and used following

```
gfortran -o C3_pes.x C3_pes.f90
./C3_pes.x < C3_pes_refined.input
```

to compute potential energies in cm^{-1} for the bond-angles and bond-lengths listed in Lines 62–72 of the input file; $^{12}C_3$ potential energies listed in the same lines should agree with those computed to the digit.

Please note: Oxford University Press is not responsible for the content or functionality of any supporting materials supplied by the authors. Any queries (other than missing material) should be directed to the corresponding author for the article.

ACKNOWLEDGEMENTS

The authors are indebted to Marie-Aline Martin-Drumel for a machine-readable copy of her C_3 infrared spectrum covering the frequency range 1900–2100 cm^{-1}. This work used the DiRAC Data Intensive service (CSD3) at the University of Cambridge, managed by the University of Cambridge University Information Services and the DiRAC Data Intensive service (DIaL2) at the University of Leicester, managed by the University of Leicester Research Computing Service on behalf of the STFC DiRAC HPC Facility (www.dirac.ac.uk). The DiRAC services at Cambridge and Leicester were funded by BEIS, UKRI, and STFC capital funding and STFC operations grants. Computing facilities at University College London and the University of Oxford were also used. This work was supported by the STFC Project No. ST/Y001508/1 and by the European Research Council (ERC) under the European Union's Horizon 2020 research and innovation programme through Advance Grant number 883830. NFZ also acknowledges support by State Project IAPRAS No. FFUF-2024-0016.

DATA AVAILABILITY

As with other ExoMol line lists, our energy levels (states file), line lists in the form of Einstein A-Coefficients (trans file), calculated partition functions and opacities are available in the ExoMol data base (www.exomol.com). Our refined version of the Schröder & Sebald (2016) PES for $^{12}C_3$ has been included in tabular form, along with a FORTRAN90 subroutine for reading it, as supplementary material.

REFERENCES

Al-Refaie A. F., Changeat Q., Waldmann I. P., Tinetti G., 2021, ApJ, 917, 37
Asplund M., Nordlund Å., Trampedach R., Allende Prieto C., Stein R. F., 2000, A&A, 359, 729
Blackwell D. E., Booth A. J., Petford A. D., 1984, A&A, 132, 236
Bowesman C. A. et al., 2023, MNRAS, 519, 6333
Brady R. P., Yurchenko S. N., Tennyson J., Kim G.-S., 2024, MNRAS, 527, 6675
Breier A. A. et al., 2016, J. Chem. Phys., 145, 234302
Bunker P. R., Jensen P., 1998, Molecular Symmetry and Spectroscopy, 2 edn. NRC Research Press, Ottawa
Chubb K. L. et al., 2021, A&A, 646, A21
Clayton G. C., 1996, PASP, 108, 225
Cooley J. W., 1961, Math. Comp., 15, 363
Douglas A. E., 1951, ApJ, 114, 466
Fan H. et al., 2024, A&A, 681, A6
Furtenbacher T., Császár A. G., Tennyson J., 2007, J. Mol. Spectrosc., 245, 115
Gausset L., Herzberg G., Lagerqvist A., Rosen B., 1965, ApJ, 142, 45
Gautschy-Loidl R., Höfner S., Jørgensen U. G., Hron J., 2004, A&A, 422, 289
Gendriesch R., Pehl K., Giesen T., Winnewisser G., Lewen I. F., 2003, Z. Naturforsch, 58, 129
Giesen T. F., Van Orden A. O., Cruzan J. D., Provencal R. A., Saykally R. J., Gendriesch R., Lewen F., Winnewisser G., 2001, ApJ, 551, L181
Giesen T. F., Mookerjea B., Fuchs G. W., Breier A. A., Witsch D., Simon R., Stutzki J., 2020, A&A, 633, A120
Gilra D. P., 1973, in Greenberg J. M., van de Hulst H. C., eds, Proc. IAU Symp. 52, Interstellar Dust and Related Topics. Reidel, Dordrecht, p. 517
Goulay F., Nemes L., Schrader P. E., Michelsen H. A., 2010, Mol. Phys., 108, 1013
Guilluy G., Sozzetti A., Brogi M., Bonomo A. S., Giacobbe P., Claudi R., Benatti S., 2019, A&A, 625, A107
Hébrard E., Dobrijevic M., Loison J. C., Bergeat A., Hickson K. M., Caralp F., 2013, A&A, 552, A132
Hinkle K. W., Keady J. J., Bernath P. F., 1988, Science, 241, 1319
Höfner S., Gautschy-Loidl R., Aringer B., Jørgensen U. G., 2003, A&A, 399, 589
Honig R. E., 1954, J. Chem. Phys., 22, 126
Huggins W., 1881, Proc. R. Soc, 33, 1
Irwin A. W., 1981, ApJS, 45, 621
Irwin P. G. J. et al., 2008, J. Quant. Spectrosc. Radiat. Transf., 109, 1136
Jørgensen U. G., 1997, in van Dishoek E. F., ed, Proc. IAU Symp. 178, Molecules in Astrophysics. Kluwer, Dordrecht, p. 441
Jørgensen U. G., Almlöf J., Siegbahn P. E. M., 1989, ApJ, 343, 554
Kameswara Rao N., Giridhar S., Ashoka B. N., 1990, MNRAS, 244, 29
Krieg J. et al., 2013, J. Phys. Chem., 117, 3332
Lacis A. A., Oinas V., 1991, J. Geophys. Res., 96, 9027
Lagarde N. et al., 2024, A&A, 684, A70
Loison J.-C., Wakelam V., Hickson K. M., Bergeat A., Mereau R., 2014, MNRAS, 437, 930
Lombardo N. A. et al., 2019, ApJ, 881, L33
Marigo P., Aringer B., Girardi L., Bressan A., 2022, ApJ, 940, 129
Martin-Drumel M.-A. et al., 2023, J. Mol. Spectrosc., 391, 111734
McBride B. J., Heimel S., Ehlers J. G., Gordon S., 1963, NASA SP-3001, 3001
McKellar A., 1948, ApJ, 108, 453
Mellor T. M., Yurchenko S. N., Jensen P., 2021, Symmetry, 13, 548
Mellor T., Owens A., Tennyson J., Yurchenko S. N., 2023, MNRAS, 520, 1997
Min M., Ormel C. W., Ormel C. W., Chubb K., Helling C., Kawashima Y., 2020, A&A, 642, A28
Moazzen-Ahmadi N., McKellar A. R. W., 1993, J. Chem. Phys., 98, 7757
Molliére P., Wardenier J. P., van Boekel R., Henning T., Molaverdikhani K., Snellen I. A. G., 2019, A&A, 627, A67
Neale L., Tennyson J., 1995, ApJ, 454, L169
Noumerov B. V., 1924, MNRAS, 84, 592
Owens A., Tennyson J., Yurchenko S. N., 2021, MNRAS, 502, 1128
Owens A., Dooley S., McLaughlin L., Tan B., Zhang G., Yurchenko S. N., Tennyson J., 2022a, MNRAS, 511, 5448
Owens A., Mitrushchenkov A., Yurchenko S. N., Tennyson J., 2022b, MNRAS, 516, 3995
Owens A., Wright S. O. M., Pavlenko Y., Mitrushchenkov A., Koput J., Yurchenko S. N., Tennyson J., 2024a, MNRAS, 527, 731
Owens A., Yurchenko S. N., Tennyson J., 2024b, MNRAS, 530, 4004
Pearce O., Yurchenko S. N., Tennyson J., 2024, MNRAS, 527, 10726
Pitzer K. S., Clementi E., 1959, Univ. California, California
Rianço-Silva R., Machado P., Martins Z., Lellouch E., Loison J.-C., Dobrijevic M., Dias J. A., Ribeiro J., 2024, Planet. Space Sci., 240, 105836
Rocha C. M. R., Varandas A. J. C., 2015, J. Chem. Phys., 143, 074302
Rocha C. M. R., Varandas A. J. C., 2018, Phys. Chem. Chem. Phys., 20, 10319
Schröder B., Sebald P., 2016, J. Chem. Phys., 144, 044307
Schuurman M. S., Stolow A., 2018, Ann. Rev. Phys. Chem., 69, 427
Semenov M., Clark N., Yurchenko S. N., Kim G.-S., Tennyson J., 2022, MNRAS, 516, 1158
Seo Y. M. et al., 2019, ApJ, 871, 134
Sweigart A. V., Greggio L., Renzini A., 1989, ApJS, 69, 911
Swings P., McKellar A., Rao K. N., 1953, MNRAS, 113, 571
Tennyson J., 2024, Mol. Phys., 122, e2276912
Tennyson J., Yurchenko S. N., 2012, MNRAS, 425, 21
Tennyson J., Yurchenko S. N., 2018, Atoms, 6, 26
Tennyson J., Furtenbacher T., Yurchenko S. N., Császár A. G., 2024a, J. Quant. Spec. Radiat. Transf., 316, 108902
Tennyson J. et al., 2024b, J. Quant. Spectrosc. Radiat. Transf., 326, 109083
Treffers R. R., Gilra D. P., 1975, ApJ, 202, 839
Tsuji T., 1964, Proc. Japan Acad. B, 40, 99
Weltner William J., McLeod Donald J., 1964, J. Chem. Phys., 40, 1305
Weltner W. J., Walsh P. N., Angell C. L., 1964, J. Chem. Phys., 40, 1299
Worth G. A., Cederbaum L. S., 2004, Ann. Rev. Phys. Chem., 55, 127
Yarkony D. R., 1996, Rev. Mod. Phys., 68, 985
Yurchenko S., 2023, Computational Spectroscopy of Polyatomic Molecules. CRC Press, Florida
Yurchenko S. N., Mellor T. M., 2020, J. Chem. Phys., 153, 154106
Yurchenko S. N., Thiel W., Jensen P., 2007, J. Mol. Spectrosc., 245, 126
Yurchenko S. N., Yachmenev A., Ovsyannikov R. I., 2017, J. Chem. Theory Comput., 13, 4368
Yurchenko S. N., Al-Refaie A. F., Tennyson J., 2018, A&A, 614, A131
Yurchenko S. N., Mellor T. M., Freedman R. S., Tennyson J., 2020, MNRAS, 496, 5282
Yurchenko S. N. et al., 2022, MNRAS, 510, 903
Yurchenko S. N., Nogué E., Azzam A. A. A., Tennyson J., 2023, MNRAS, 520, 5183
Yurchenko S. N., Owens A., Kefala K., Tennyson J., 2024a, MNRAS, 528, 3719
Yurchenko S. N., Brady R. P., Tennyson J., Smirnov A. N., Vasilyev O. A., Solomonik V. G., 2024b, MNRAS, 527, 4899
Yurchenko S. N. et al., 2024c, MNRAS, 527, 9736
Yurchenko S. N., Mellor T., Tennyson J., 2024d, MNRAS, 534, 1364
Zhang J., Hill C., Tennyson J., Yurchenko S. N., 2024, ApJS

This paper has been typeset from a TEX/LATEX file prepared by the author.